Publishing Excellence
Inspiring Progress
ARISTON PUBLICATIONS
ChemSci Advances
ISSN: 2997-9587 www.aristonpubs.com/chemsci-advances https://doi.org/10.69626/csa.2025.0314

RESEARCH ARTICLE

A Green and Sustainable Microwave–Assisted Protocol for the Synthesis of Tetrahydrobenzo[b]pyran Derivatives Using Mn_3O_4 Nanoparticles as a Heterogeneous Catalyst

Pratik A. Patil [1], Pravin A. Shinde [1], Paresh S. Gaikar [1], Gayatri S. Bhagwat [2], Priya A. Patil [3], Prachi A. Patil [1], Pallavi S. Tathe [4], Sarang R. Bhagwat [1,*]

ABSTRACT: This study establishes an environmentally benign and highly efficient method for synthesizing pharmaceutically relevant 2-amino-5-oxo-5,6,7,8-tetrahydro-4H-benzo[b]pyran derivatives. The process employs a one-pot, three-component condensation of dimedone, malononitrile, and various aromatic aldehydes, catalyzed by manganese oxide (Mn_3O_4) nanoparticles under microwave irradiation. Reaction parameters, including solvent selection and catalyst loading, were systematically optimized. Ethanol emerged as the superior solvent, enabling excellent product yields within short reaction times. The Mn_3O_4 nanoparticles functioned as a robust, reusable, and magnetically separable heterogeneous catalyst, exhibiting outstanding activity and stability throughout the reaction cycles. This approach aligns with green chemistry principles by eliminating toxic solvents, reducing energy consumption through microwave assistance, and offering high atom economy. All synthesized compounds were obtained in high purity and yield, as confirmed by spectroscopic techniques. The developed protocol represents a sustainable, scalable, and economically viable alternative to conventional methods for accessing oxygen-containing heterocycles, with significant potential in medicinal and synthetic chemistry applications.

Keywords: Green synthesis, Microwave irradiation, Heterogeneous catalysis, Mn_3O_4 nanoparticles, Tetrahydrobenzo[b]pyran, Multicomponent reaction

Received: 24 June 2025; Revised: 29 August 2025; Accepted: 27 October 2025; Published Online: 19 November 2025

[1] Rayat Shikshan Sanstha's, Karmaveer Bhaurao Patil College, Vashi, Navi Mumbai, 400703, Maharashtra, India.
[2] Mahatma Phule A.S.C. College, Panvel, Raigad, 410206, Maharashtra, India.
[3] Changu Kana Thakur A. C. S. College, New Panvel, 410206, Maharashtra, India.
[4] Chandmal Tarachand Bora College, Shirur affiliated to Savitribai Phule Pune, Maharashtra, India.

* Author to whom correspondence should be addressed: saarang012@gmail.com (Sarang R. Bhagwat)

1. INTRODUCTION

The field of nanoscience has witnessed transformative growth over recent decades, fundamentally altering approaches across chemistry, materials science, and medicine. A cornerstone of this advancement is the synthesis and application of metal oxide nanoparticles, which exhibit a remarkable array of distinctive physicochemical properties not found in their bulk counterparts [1]. These properties, including high surface area to volume ratios, quantum confinement effects, and unique electronic structures, have

© Ariston Publications 2025. All rights reserved.

unlocked extensive applications in areas ranging from electronics and energy storage to environmental remediation and catalysis. Within this broad landscape, manganese oxide nanoparticles, particularly in the form of Mn_3O_4 (hausmannite), have garnered significant and sustained interest from the scientific community. This interest stems from a compelling combination of factors: their ability to seamlessly transition between multiple oxidation states (Mn^{2+}, Mn^{3+}), their natural abundance and associated low cost, and their documented low toxicity, which collectively render them an environmentally benign and economically attractive nanomaterial [2]. Consequently, Mn_3O_4 nanoparticles have been successfully deployed in diverse roles, including as components in high-performance battery electrodes, agents for the catalytic degradation of pollutants, sensitive elements in chemical sensors, and, most pertinently for this work, as highly efficient catalysts for organic transformations [3].

The method employed for synthesizing these nanoparticles is critical, as it directly governs their size, morphology, crystallinity, and ultimately, their functional efficacy. Among the various techniques available, microwave-assisted synthesis has emerged as one of the most modern and effective strategies for the fabrication of Mn_3O_4 nanoparticles [4]. This technique offers profound advantages over conventional heating methods, such as oil baths or mantles, which rely on slow conductive and convective heat transfer. In contrast, microwave irradiation delivers energy directly to polar molecules or ionic reactants within the reaction medium through dipole rotation and ionic conduction, resulting in rapid, uniform, and volumetric heating [6]. This direct energy transfer mechanism leads to substantially faster reaction kinetics, significantly reduced processing times, and lower overall energy consumption. Furthermore, the homogeneous heating environment suppresses local thermal gradients, which often lead to irregular particle growth, thereby yielding products with superior uniformity in size and shape, higher crystallinity, and controlled morphological features [5, 7]. The accelerated nucleation and growth kinetics under microwaves facilitate the formation of monodisperse, well-defined nanocrystals, making this approach ideal for producing high-quality catalytic materials.

The catalytic utility of Mn_3O_4 nanoparticles has become increasingly prominent in modern organic synthesis, especially within the paradigm of green chemistry which emphasizes atom economy, energy efficiency, and the avoidance of hazardous substances. A particularly valuable application lies in the construction of oxygen-containing heterocycles, a vast and immensely important class of cyclic compounds where at least one atom in the ring is oxygen. These heterocyclic frameworks are ubiquitous structural motifs in molecules of profound significance across multiple disciplines. In pharmaceutical and medicinal chemistry, they form the core of numerous drugs and bioactive agents; in agrochemicals, they are key constituents of pesticides and herbicides; and in materials science, they contribute to polymers, dyes, and electronic materials [8]. Specific classes such as pyrans, furans, coumarins, and chromenes are especially notable, exhibiting a broad spectrum of documented biological activities including potent anti-inflammatory, antimicrobial, anticancer, and antioxidant effects [9]. Therefore, developing efficient, sustainable, and general methods for their synthesis is not merely an academic exercise but a necessity with direct implications for human health and technology.

Mn_3O_4 nanoparticles serve as exemplary heterogeneous catalysts for such syntheses due to their intrinsic redox activity and Lewis acidity, which enable them to facilitate key steps in oxidative transformations, cyclization reactions, and one-pot multicomponent condensations [10, 11]. Their heterogeneous nature is a major practical benefit, allowing for straightforward separation from the reaction mixture via filtration or magnetic means, and subsequent reuse without a dramatic loss of activity, which enhances the process's economic and environmental profile [12]. When the inherent catalytic prowess of Mn_3O_4 nanoparticles is coupled with the efficiency of microwave irradiation, a synergistic effect is observed. The combined system demonstrates markedly enhanced catalytic activity, leading to dramatic accelerations in reaction rates, improved product yields, and often greater selectivity, all while maintaining minimal energy and solvent usage [3, 5, 10]. This confluence of attributes makes microwave-assisted, nanoparticle-catalyzed pathways highly attractive for sustainable synthesis.

The novelty of the present work lies in the integration of a green, microwave-synthesized Mn_3O_4 nanocatalyst into a one-pot, three-component protocol specifically for the synthesis of 2-amino-5-oxo-5,6,7,8-tetrahydro-4H-benzo[b]pyran derivatives, employing ethanol as a benign solvent and optimizing the system for both efficiency and environmental compatibility.

This study demonstrates that the microwave-aided synthesis of manganese oxide nanoparticles provides a direct and eco-conscious route to high-performance catalysts. Their subsequent application in constructing pharmacologically relevant oxygen-containing heterocycles underscores their practical significance in modern synthetic methodology. This approach offers a feasible and robust pathway for achieving chemical transformations that are not only expedited and high-yielding but also align with the critical principles of cleaner and more sustainable chemistry, presenting a viable alternative to traditional, often wasteful, synthetic strategies.

2. EXPERIMENTAL DETAILS

All chemical reagents and solvents, including manganese(II) acetate tetrahydrate, dimedone, malononitrile, and the aromatic aldehydes, were of analytical grade, procured from Merck, and were used without further purification. Deionized water was used throughout the experiments. Reactions were monitored by analytical thin-layer chromatography (TLC) on pre-coated silica gel 60 F_{254} plates. Purification of the synthesized heterocyclic compounds was achieved via flash column chromatography using silica gel (Merck, 230–400

© Ariston Publications 2025. All rights reserved.

mesh) as the stationary phase with appropriate eluents. The structural identity and purity of all organic products were confirmed using spectroscopic techniques. ^1H and ^{13}C Nuclear Magnetic Resonance (NMR) spectra were acquired on a Bruker DRX400 Avance spectrometer operating at 400 MHz and 100 MHz, respectively. Dimethyl sulfoxide-d_6 (DMSO-d_6) was used as the solvent with tetramethylsilane (TMS) as an internal standard. Data are reported as chemical shift (δ, ppm), multiplicity, coupling constant (J, Hz), and integrated proton count. Melting points were determined using an electrothermal melting point apparatus in open capillaries and are reported uncorrected. Infrared (IR) spectra were recorded on an ATR-FTIR spectrometer.

2.1. Preparation of Plant Extract

An aqueous extract of *Azima tetracantha* leaves was prepared to act as a natural complexing and stabilizing agent in the nanoparticle synthesis. Fresh leaves were thoroughly washed with tap water followed by deionized water to remove surface impurities. The cleaned leaves were air-dried, then finely pulverized using a mechanical grinder. Approximately 10 grams of the resulting leaf paste was added to 100 mL of distilled water. This mixture was stirred vigorously on a magnetic stirrer at ambient temperature for 60 minutes to facilitate the extraction of phytochemicals. The crude mixture was then centrifuged at 4000 rpm for 10 minutes to sediment particulate matter. The clear supernatant was subsequently filtered through Whatman No. 1 filter paper. The final extract was stored at 4°C for use in the subsequent synthesis.

2.2. Synthesis of Mn_3O_4 Nanoparticles

Manganese oxide (Mn_3O_4) nanoparticles were synthesized via a green, microwave-assisted co-precipitation method, adapted from literature with modifications [13]. In a standard procedure, 100 mL of a 0.1 M aqueous solution of manganese(II) acetate tetrahydrate was combined with an equal volume (100 mL) of the freshly prepared *Azima tetracantha* leaf extract in a 250 mL round-bottom flask under continuous stirring for 10 minutes. The pH of the resulting mixture was then adjusted to approximately 10 by the dropwise addition of a 1 M sodium hydroxide (NaOH) solution, which induced the formation of a brown precipitate. The reaction vessel was then subjected to microwave irradiation in a domestic microwave oven at a power of 800 W for 30 minutes. The resulting brown product was isolated by centrifugation at 3000 rpm, washed exhaustively with distilled water and absolute ethanol to remove ionic and organic residues, and dried overnight in a hot air oven at 80°C. The dried powder was finally calcined in a muffle furnace at 450°C for 2 hours to obtain the crystalline Mn_3O_4 nanoparticles.

2.3. General Procedure for the Synthesis of 2-Amino-5-oxo-5,6,7,8-tetrahydro-4H-benzo[b]pyran Derivatives

The catalytic activity of the synthesized Mn_3O_4 nanoparticles was evaluated in a one-pot, three-component condensation reaction. In a typical experiment, a mixture of dimedone (1 mmol), malononitrile (1 mmol), and an aromatic aldehyde (1 mmol) was combined with Mn_3O_4 nanoparticles (10 mg) in a conical flask. Absolute ethanol (3 mL) was added as the reaction medium. The vessel was placed in a microwave reactor and irradiated at a fixed temperature of 80°C. The reaction progress was monitored at intervals by TLC using a mixture of n-hexane and ethyl acetate (7:3 v/v) as the mobile phase. Upon completion, the reaction mixture was poured into ice-cold distilled water (20 mL). The precipitated solid product was collected by vacuum filtration. The heterogeneous catalyst remained on the filter paper and was recovered. The crude product was purified by recrystallization from hot ethanol to yield the pure tetrahydrobenzo[b]pyran derivative.

2.4. Catalytic Reaction Optimization Studies

To establish the optimal reaction conditions, initial optimization was performed using p-nitrobenzaldehyde as a model substrate. The influence of the solvent was studied by conducting the reaction in water, ethanol, methanol, and dichloromethane, keeping other parameters constant. Subsequently, the effect of catalyst loading was investigated by varying the amount of Mn_3O_4 nanoparticles from 0 to 20 mg while using the optimal solvent. The reaction time and yield were the primary metrics for evaluation.

2.5. Characterization Techniques for Mn_3O_4 Nanoparticles

The synthesized Mn_3O_4 nanoparticles were characterized using several analytical techniques to determine their physicochemical properties. X-ray diffraction (XRD) analysis was conducted on a Bruker D8 Advance diffractometer equipped with Cu Kα radiation (λ = 1.5406 Å) to identify the crystalline phase and structure. Data were collected over a 2θ range of 10° to 80°. Optical properties were analyzed by UV-Visible spectroscopy using a Shimadzu UV-2600 spectrophotometer, with measurements taken in the wavelength range of 200 to 800 nm. The surface morphology and particle size of the nanoparticles were examined using a ZEISS EVO 18 scanning electron microscope (SEM) operated at an accelerating voltage of 5 kV.

3. RESULTS AND DISCUSSION

The successful synthesis and application of manganese oxide (Mn_3O_4) nanoparticles as a heterogeneous catalyst for the formation of biologically relevant heterocycles form the core

© Ariston Publications 2025. All rights reserved.

of this investigation. This section systematically presents the characterization of the synthesized nanocatalyst, the optimization of the reaction parameters for the model transformation, and the evaluation of the substrate scope alongside comprehensive spectroscopic validation of the final products.

3.1. Structural and Crystalline Phase Analysis (XRD)

The crystalline structure and phase purity of the synthesized nanoparticles were unequivocally determined using X-ray diffraction (XRD) analysis. The obtained diffractogram, presented in **Figure 1(a)**, displays a series of sharp and well-defined diffraction peaks. These peaks were observed at 2θ values of 18.1°, 29.0°, 31.2°, 32.4°, 36.2°, 38.2°, 44.5°, 50.9°, 54.0°, 56.1°, 58.7°, 60.0°, and 64.8°. These reflections are systematically indexed to the crystallographic planes (101), (112), (200), (103), (211), (004), (220), (105), (312), (303), (321), (224), and (400), respectively. The positions and relative intensities of all peaks exhibit an excellent match with the standard reference pattern for hausmannite-phase Mn_3O_4 (JCPDS card no. 24-0734). The absence of any extraneous peaks corresponding to other manganese oxides (such as MnO or MnO_2) or precursor salts confirms the high phase purity of the product. The sharpness of the peaks indicates a high degree of crystallinity, which is a direct benefit of the microwave-assisted synthesis route, promoting rapid and homogeneous nucleation and growth [7]. This confirmed monoclinic Mn_3O_4 structure is particularly advantageous for catalysis, as it provides a stable framework with accessible Mn^{2+} and Mn^{3+} sites capable of redox and Lewis acid catalytic cycles [11].

3.2. Optical Properties Analysis (UV-Vis Spectroscopy)

The optical characteristics of the prepared nanoparticles were probed using UV-Visible absorption spectroscopy across a wavelength range of 200 to 800 nm, as shown in **Figure 1(b)**. The spectrum is dominated by a strong and distinct absorption maximum centered at approximately 365 nm. This prominent absorption band is a signature feature of Mn_3O_4 and is attributed to a ligand-to-metal charge transfer (LMCT) transition involving the oxygen (2p) and manganese (3d) orbitals within the Mn–O bonds of the crystal lattice. The presence of this well-defined peak, with no significant absorption in the visible region, corroborates the XRD findings and confirms the formation of Mn_3O_4 nanoparticles. Furthermore, the position and nature of this absorption edge are indicative of the material's semiconducting properties. The substantial absorption in the UV region suggests a wide bandgap, which is characteristic of Mn_3O_4 and relates to its electronic structure. This property, while not directly exploited in the present thermal catalytic reaction, underscores the material's potential for photo-assisted catalytic applications [3].

3.3. Morphological and Surface Analysis (SEM)

The surface morphology, particle size, and structural arrangement of the synthesized Mn_3O_4 nanoparticles were examined using scanning electron microscopy (SEM). The micrographs, presented in **Figure 2** at two different magnifications, reveal critical insights into the catalyst's physical form. The images confirm the successful formation of nanostructures with a predominantly spherical or near-spherical morphology. The particles demonstrate a reasonably uniform size distribution, although a degree of agglomeration is observable. This agglomeration is a common phenomenon in nanomaterials and is primarily driven by the minimization of surface energy. Importantly, the particles appear well-crystallized and are interconnected, forming a porous, three-dimensional network. This porous architecture is highly beneficial for catalytic applications as it results in a high surface-to-volume ratio, thereby providing a large number of active sites for reactant molecules to adsorb and react. The homogeneous surface texture observed across the sample suggests consistent synthesis conditions, which is vital for reproducible catalytic performance [12].

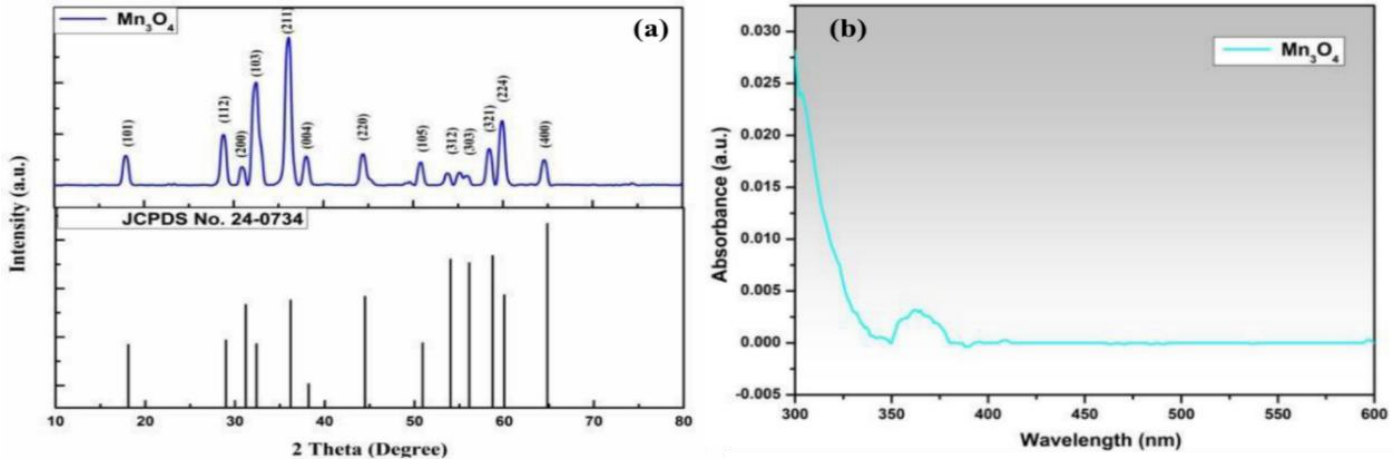


Fig. 1. Typical (a) XRD pattern, and (b) UV-visible spectrum of Mn_3O_4 nanoparticles.

© Ariston Publications 2025. All rights reserved.

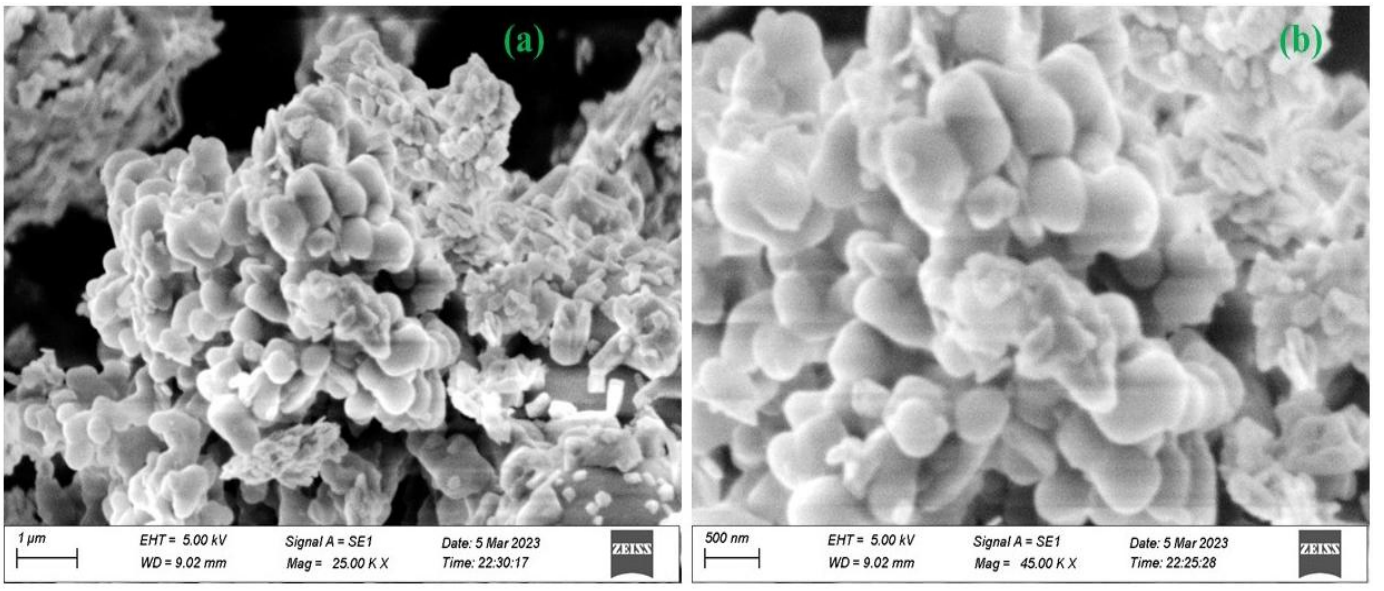


Fig. 2. (a) Low, and (b) high-magnification SEM images of Mn_3O_4 nanoparticles.

3.4. Optimization of Catalytic Reaction Conditions

To maximize the efficiency of the one-pot, three-component synthesis of 2-amino-5-oxo-5,6,7,8-tetrahydro-4H-benzo[b]pyran, a systematic optimization of reaction parameters was undertaken using p-nitrobenzaldehyde as a model substrate.

3.4.1. Solvent Screening

The choice of solvent is critical, influencing reaction rate, yield, and adherence to green chemistry principles. As summarized in **Table 1**, four different solvents were evaluated: water, ethanol, methanol, and dichloromethane (CH_2Cl_2). The reaction proceeded efficiently in all protic solvents, with water and methanol affording a 91% yield in 5 minutes. Ethanol, however, proved to be the optimal medium, delivering a slightly higher yield of 93% in a reduced time of 4 minutes. This superior performance can be attributed to ethanol's ideal polarity, which effectively solubilizes both the organic reactants and the inorganic nanoparticle catalyst, facilitating efficient interaction. In contrast, the aprotic solvent dichloromethane resulted in a longer reaction time (7 minutes) and a lower yield (87%), likely due to poor dispersion or interaction with the polar catalyst surface. Consequently, ethanol was selected as the preferred green solvent for all subsequent reactions, balancing performance with environmental benignity [10].

3.4.2. Catalyst Loading Optimization

The influence of Mn_3O_4 nanoparticle loading on the model reaction was investigated, and the results are presented in **Table 2**. A control experiment conducted in the absence of any catalyst yielded the product in 89% after a prolonged reaction time of 7 minutes, indicating that the reaction can proceed thermally but is inefficient. The introduction of just 5 mg of catalyst dramatically improved the kinetics, reducing the time to 4 minutes and increasing the yield to 93%. Increasing the catalyst amount to 10 mg resulted in the best performance, achieving an excellent yield of 96% in merely 2 minutes. A further increase to 20 mg did not enhance the yield or reduce the time, suggesting that the active sites are saturated at the 10 mg loading. This identifies 10 mg as the optimal catalyst quantity, providing maximum efficiency without wasteful excess, which is a key economic and environmental consideration for sustainable processes.

Table 1. Effect of different solvents on the reaction of dimedone and malononitrile with p-nitro benzaldehyde.

S. No.	Solvent	Reaction time	Yield
1.	Water	5	91
2.	Ethanol	4	93
3.	Methanol	5	91
4.	CH_2Cl_2	7	87

3.5. Substrate Scope and Reaction Scope Evaluation

With the optimized conditions established (10 mg Mn_3O_4, ethanol, microwave irradiation at 80°C), the generality and efficiency of the catalytic protocol were explored using a variety of aromatic aldehydes bearing diverse electronic substituents. The results are compiled in **Table 3**. The protocol demonstrated remarkable versatility and high efficiency across the board. Aromatic aldehydes containing

© Ariston Publications 2025. All rights reserved.

strong electron-withdrawing groups (EWGs) such as nitro (entries 1-2), chloro (entry 3), and bromo (entry 4) reacted with exceptional speed, furnishing the corresponding tetrahydrobenzo[b]pyran derivatives in excellent yields of 95-97% within 2-3 minutes. The enhanced reactivity of EWG-bearing aldehydes is consistent with their increased electrophilicity at the carbonyl carbon, facilitating the initial nucleophilic attack step in the multicomponent cascade.

Table 2. Effects of different amounts of catalyst on the reaction of dimedone and malononitrile with p-nitro benzaldehyde.

S. No.	Catalyst (mol%)	Reaction time (min)	Yield (%)
1.	No catalyst	7	89
2.	5 mg	4	93
3.	10 mg	2	96
4.	20 mg	2	96

*Reaction conditions: p-nitrobenzaldehyde (1 mmol), dimedone (1 mmol), and malononitrile (1 mmol), solvent-ethanol.

Aldehydes substituted with electron-donating groups (EDGs) like hydroxy (entries 5-6) were also competent substrates, yielding the desired products in high yields of 94-95%. However, as anticipated, these reactions required slightly longer times (4-5 minutes) compared to their electron-deficient counterparts due to the reduced electrophilicity of the carbonyl group. Notably, the position of the substituent also had a minor effect, with ortho-substituted aldehydes (entries 2 and 6) taking marginally longer than their para-isomers (entries 1 and 5), which can be rationalized by steric hindrance near the reaction center. The consistent high yields and short reaction times for all tested aldehydes, regardless of their electronic nature, underscore the robust and highly active nature of the Mn_3O_4 nanocatalyst under microwave irradiation. **Figure 3** illustrates the general reaction scheme for the one-pot, three-component synthesis of 2-amino-5-oxo-5,6,7,8-tetrahydro-4H-benzo[b]pyran derivatives (**a–f**). The reaction proceeds via the condensation of an aromatic aldehyde, dimedone, and malononitrile, catalyzed by Mn_3O_4 nanoparticles under microwave irradiation at 80°C. This efficient and green methodology facilitates the rapid construction of the heterocyclic framework in a single step.

3.6. Spectral data of derivatives of 2-amino-5-oxo-5,6,7,8-tetrahydro-4H-benzo[b]pyran

As shown in Table 3, we studied the reaction with an extensive range of aromatic aldehydes, including electron-donating and electron-withdrawing groups. Both electron-rich and electron-deficient aldehydes performed well and produced large yields of products when exposed to microwaves. Electron-deficient aldehydes produced excellent yields of the corresponding products in shorter reaction times (Table 3, entries 1-4), whereas aromatic aldehydes with substituents that donate electrons carried out the reaction at longer reaction times (Table 3, entries 5-6), resulting in lower yields of the corresponding tetrahydrobenzo[b]pyrans.

3.7. FTIR, ^{1}H-NMR, and ^{13}C-NMR for the synthesized compounds (a-f)

3.7.1. 2-amino-7,7-dimethyl-4-(4-nitrophenyl) -5-oxo-5,6,7,8-tetrahydro-4H-chromene-3-carbonitrile (a)

Yellow solid, yield: 96%, M.P.: 180°C; IR (ATR, cm^{-1}): 3320 NH_2, 1140 C-N, 2190 CN, 1515 C=C, 1601 C=O, 1101 C-O, 2965 CH.

^{1}H NMR (400 MHz, DMSO-d6): δ(ppm) 8.16-8.18 (d, J=7.12 Hz, 2H, ArH). 7.44-7.45 (d, J= 5.36, 2H, ArH), 7.19 (d, 2H, NH_2), 4.37 (s, 1H, Ar-CH), 2.55 (t, J= 3.52 Hz, 2H, CH_2), 2.26 (d, J= 16.08 Hz, 1H, CH_2), 2.12 (d, J= 16.04 Hz, 1H, CH_2), 1.05 (s, 3H, CH_3), 0.97 (s, 3H, CH_3).

13C NMR (DMSO-d6, 100 MHz) δ: 27.3, 28.7, 32.2, 36.0, 50.2, 57.4, 112.1, 119.7, 124.1, 129.0, 146.7, 152.74, 159.0, 163.5, 196.1.

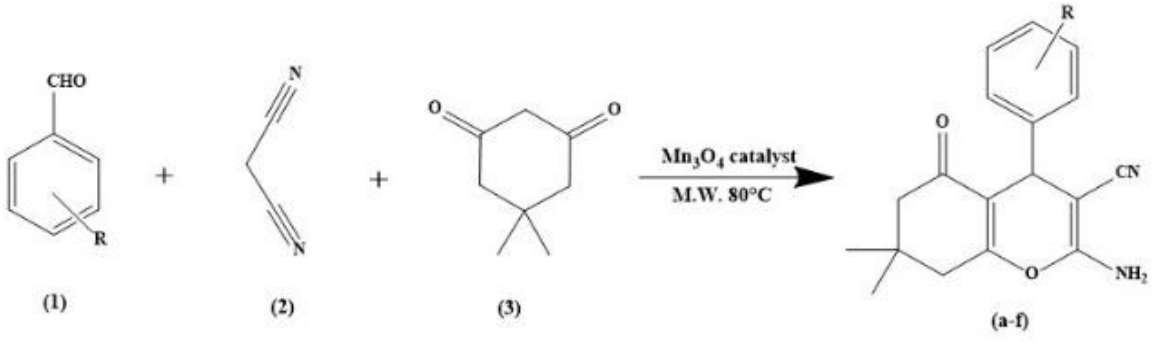


Fig. 3. General reaction scheme for the Mn_3O_4-catalyzed synthesis of 2-amino-5-oxo-5,6,7,8-tetrahydro-4H-benzo[b]pyran derivatives under microwave irradiation.

© Ariston Publications 2025. All rights reserved.

Table 3. Synthesis of derivatives of 2-amino-5-oxo-5,6,7,8-tetrahydro-4H-benzo[b]pyran in the presence of Mn_3O_4.

S. No.	Ar	Product	Time (min.)	Yield (%)	M.P. (˚C) Observed	M.P. (˚C) Actual
1.	4-NO_2-C_6H_4	a	2	96	180	179-181
2.	2-NO_2-C_6H_4	b	3	95	238	237-238
3.	4-Cl-C_6H_4	c	3	96	212	212-213
4.	4-Br-C_6H_4	d	2	97	200	200-201
5.	4-OH-C_6H_4	e	4	95	226	225-227
6.	2-OH-C_6H_4	f	5	94	176	175-177

3.7.2. 2-amino-7,7-dimethyl-4-(2-nitrophenyl)-5-oxo-5,6,7,8-tetrahydro-4H-chromene-3-carbonitrile (b)

Yellow solid, yield: 95%; M.P.: 238°C; IR (ATR, cm^{-1}): 3328 NH_2, 1142 C-N, 2192 CN, 1521 C=C, 1592 C=O, 1040 C-O, 2959 CH.

^{1}H-NMR (400 MHz, DMSO-d6): δ(ppm) 7.60-7.64 (t, J= 7.56 Hz, 1H, ArH), 7.38-7.41 (t, J= 7.76 Hz, 2H, ArH), 0.83 (s, 3H, CH3), 7.06 (d, J= 7.8 Hz, 2H, NH2), 4.89 (s, 1H, Ar-CH), 0.97 (s, 3H, CH3), 2.50 (m, 2H, CH2), 2.15-2.19 (d, J= 16.12 Hz, 1H, CH2), 1.94-1.99 (d, J= 16.12 Hz, 1H, CH2).

13C NMR (DMSO-d6, 100 MHz) δ: 27.3, 28.7, 32.2, 36.0, 50.2, 57.4, 112.1, 119.7, 124.1, 129.0, 146.7, 152.74, 159.6, 163.1, 196.3.

3.7.3. 2-amino-4-(4-chlorophenyl) -7,7-dimethyl-5-oxo-5,6,7,8-tetrahydro-4H-chromene -3- carbonitrile (c)

White solid, yield: 96%, M.P.: 212°C; IR (ATR, cm^{-1}): 3318 NH_2, 1127 C-N, 2190 CN, 1604 C=C, 1647 C=O, 1038 C-O, 2963 CH.

^{1}H-NMR (400 MHz, DMSO-d6): δ(ppm) 7.35-7.36 (d, J= 8.16 Hz, 2H, ArH), 7.18-7.20 (d, J= 8.2 Hz, 2H, ArH), 7.05 (d, 2H, NH_2), 4.21 (s, 1H, Ar-CH), 2.52-2.57 (m, 2H, CH_2), 2.25-2.28 (d, J= 16.08 Hz, 1H, CH_2), 2.10-2.13 (d, J= 16.04 Hz, 1H, CH_2), 1.04 (s, 3H, CH_3), 0.95 (s, 3H, CH_3).

13C NMR (DMSO-d6, 100 MHz) δ: 27.7, 29.2, 32.6, 36.0, 50.8, 58.7, 112.7, 120.0, 129.5, 123.0, 131.5, 144.1, 158.9, 163.0, 196.1.

3.7.4. 2-amino-4-(4-bromophenyl)-7,7-dimethyl-5-oxo-5,6,7,8-tetrahydro-4H-chromene-3- carbonitrile (d)

White solid, yield: 97%, M.P.: 200°C; IR (ATR, cm^{-1}): 3317 NH_2, 1142 C-N, 2192 CN, 1604 C=C, 1652 C=O, 1038 C-O, 2962 CH.

^{1}H-NMR (400 MHz, DMSO-d_6): δ (ppm) 7.49-7.51 (d, J J= 8.16 Hz, 2H, ArH), 7.12-7.14 (d, J = 8.2 Hz, 2H, ArH), 7.05 (d, 2H, NH_2), 4.19 (s, 1H, Ar-CH), 2.53-2.56 (m, 2H, CH_2), 2.25-2.28 (d, J = 16.08 Hz, 1H, CH_2), 2.10-2.14 (d, J = 16.04 Hz, 1H, CH_2), 1.04 (s, 3H, CH_3), 0.96 (s, 3H, CH_3).

3.7.5. 2-amino-7,7-dimethyl-4-(4-hydroxyphenyl)-5-oxo-5,6,7,8-tetrahydro-4H-chromene-3- carbonitrile (e)

Yellow solid, Yield: 95%; M.P.: 226°C; IR (ATR, cm^{-1}): 3314 NH_2, 1143 C-N, 2193 CN, 1607 C=C, 1647 C=O, 1037 C-O, 2968 CH.

^{1}H-NMR (400 MHz, DMSO-d6): δ(ppm) 6.94-6.95 (d, J= 8.16 Hz, 2H, ArH), 6.68-6.69 (d, J= 8.2 Hz, 2H, ArH), 6.90 (s, 2H, NH_2), 4.07 (s, 1H, Ar-CH), 2.45-2.54 (m, 2H, CH_2), 2.24-2.27 (d, J= 16.08 Hz, 1H, CH_2), 2.10-2.11 (d, J= 16.04 Hz, 1H, CH_2), 1.04 (s, 3H, CH_3), 0.95 (s, 3H, CH_3).

3.7.6. 2-amino-7,7-dimethyl-4-(2-hydroxyphenyl)-5-oxo-5,6,7,8-tetrahydro-4H-chromene-3- carbonitrile (f)

Yellow solid, yield: 94%, M.P.: 176°C; IR (FTIR, cm^{-1}):): 2923 NH_2, 1140 C-N, 2198 CN, 1598 C=C, 1644 C=O, 1037 C-O, 2923 CH.

^{1}H-NMR (400 MHz, DMSO-d_6): δ(ppm) 6.96-6.97 (m, 1H, ArH), 6.70-7.71 (d, J= 8.2 Hz, 2H, ArH), 6.90 (s, 2H, NH_2), 4.09 (s, 1H, Ar-CH), 2.50-2.56 (m, 2H, CH_2), 2.25-2.28 (d, J= 16.08 Hz, 1H, CH_2), 2.09-2.13 (d, J= 16.04 Hz, 1H, CH_2), 1.05 (s, 3H, CH_3), 0.96 (s, 3H, CH_3).

All synthesized compounds (**a-f**) were purified and characterized using a combination of spectroscopic and analytical techniques to confirm their identity and purity. The melting points of the products were sharp and aligned closely with literature values, providing initial evidence of purity. Fourier-transform infrared (FTIR) spectroscopy revealed characteristic absorption bands for each functional group present. All compounds showed distinct, broad bands in the region of 3314-3328 cm^{-1} corresponding to the asymmetric and symmetric stretching vibrations of the primary amino (–NH_2) group. The sharp, intense peak in the range of 2190-

© Ariston Publications 2025. All rights reserved.

2198 cm^{-1} is a clear signature of the nitrile (–C≡N) group's stretching vibration. The carbonyl (C=O) stretching of the pyranone ring appeared as a strong band between 1592-1652 cm^{-1}, while the C–O–C ether stretch of the pyran ring was observed around 1037-1101 cm^{-1}. Aromatic and aliphatic C–H stretches were also present in the expected regions.

Definitive structural confirmation was achieved through ^1H and ^{13}C nuclear magnetic resonance (NMR) spectroscopy. The ^1H NMR spectra (recorded in DMSO-d_6) for all compounds displayed a characteristic singlet between δ 4.07-4.89 ppm, which is assigned to the methine proton (Ar–CH) at the 4-position of the pyran ring, a key diagnostic signal for the formed cyclic structure. The two methyl groups on the quaternary carbon of the dimedone moiety appeared as two distinct singlets in the region of δ 0.95-1.05 ppm. The methylene (CH_2) protons of the cyclohexenone ring resonated as complex multiplets or distinct doublets between δ 2.10-2.57 ppm. The aromatic protons of the substituted phenyl ring appeared in their expected regions and multiplicities, consistent with their substitution patterns. Furthermore, the spectra for all compounds showed a broad singlet or doublet integrating for two protons around δ 6.90-7.19 ppm, corresponding to the exchangeable protons of the $–NH_2$ group.

The ^{13}C NMR spectra provided complementary evidence, displaying signals for all distinct carbon atoms in the molecules. Key signals included the nitrile carbon at approximately δ 112-119 ppm, the carbonyl carbon of the pyranone ring at δ 196-197 ppm, and the sp^3-hybridized methine carbon (Ar–CH) around δ 50-59 ppm. The quaternary carbon bearing the two methyl groups was observed around δ 50-58 ppm, while the aromatic and olefinic carbons appeared in their characteristic regions between δ 112-163 ppm. The combined IR and NMR data are in full agreement with the proposed structures of compounds **a-f**, confirming the successful synthesis of the target 2-amino-5-oxo-5,6,7,8-tetrahydro-4H-benzo[b]pyran derivatives via the Mn_3O_4-catalyzed multicomponent reaction.

4. CONCLUSION

In summary, this work successfully demonstrates a straightforward, efficient, and environmentally conscious strategy for the preparation of tetrahydrobenzo[b]pyran derivatives. The methodology centers on a one-pot, three-component reaction facilitated by Mn_3O_4 nanoparticles as a heterogeneous catalyst under microwave irradiation in ethanol. The catalytic system offers multiple practical advantages, including ease of preparation, thermal stability, simple separation via filtration, and reusability without significant loss of activity. The use of microwave irradiation markedly accelerates the reaction, leading to high yields within minutes, while ethanol serves as a green and effective solvent. Furthermore, the process minimizes waste generation, avoids hazardous organic solvents, and requires reduced catalyst loading compared to many existing protocols. These attributes underscore the method's compatibility with the principles of green and sustainable chemistry. From an applied perspective, the approach is readily scalable and economically attractive, providing a viable pathway to synthesize biologically important heterocyclic frameworks. The ability to recover and reuse the catalyst enhances both the environmental profile and cost-effectiveness of the process. Future work may explore the extension of this catalytic system to other multicomponent transformations and the detailed investigation of the mechanistic role of Mn_3O_4 nanoparticles. Overall, this study contributes a valuable and practical tool to the synthetic chemist's repertoire, emphasizing efficiency, sustainability, and practicality in the construction of oxygen-containing heterocycles.

DECLARATIONS

Ethical Approval

We affirm that this manuscript is an original work, has not been previously published, and is not currently under consideration for publication in any other journal or conference proceedings. All authors have reviewed and approved the manuscript, and the order of authorship has been mutually agreed upon.

Funding

Not applicable

Availability of data and material

All of the data obtained or analyzed during this study is included in the report that was submitted.

Conflicts of Interest

The authors declare that they have no financial or personal interests that could have influenced the research and findings presented in this paper. The authors alone are responsible for the content and writing of this article.

Authors' contributions

All authors contributed equally in the preparation of this manuscript.

ACKNOWLEDGEMENTS

The authors gratefully acknowledge Rayat Shikshan Sanstha's Karmaveer Bhaurao Patil College, Vashi

© Ariston Publications 2025. All rights reserved.

(Autonomous), for providing financial assistance under the Seed Money Grant Scheme to support this research work.

REFERENCE

[1] Martina, K., Cravotto, G. and Varma, R.S., **2021.** Impact of microwaves on organic synthesis and strategies toward flow processes and scaling up. *The Journal of Organic Chemistry*, *86*(20), pp.13857-13872., https://doi.org/10.1021/acs.joc.1c00865

[2] Li, M., Zhang, W., Zhang, X., Lian, Y., Niu, X. and Zhu, Y., **2023.** Influences of different surface oxygen species on oxidation of toluene and/or benzene and their reaction pathways over Cu-Mn metal oxides. *Journal of Colloid and Interface Science*, *630*, pp.301-316., https://doi.org/10.1016/j.jcis.2022.10.107.

[3] Shahid, M., Katugampalage, T.R., Khalid, M., Ahmed, W., Kaewsaneha, C., Sreearunothai, P. and Opaprakasit, P., **2022.** Microwave assisted synthesis of Mn_3O_4 nanograins intercalated into reduced graphene oxide layers as cathode material for alternative clean power generation energy device. *Scientific Reports*, *12*(1), p.19043., https://doi.org/10.1038/s41598-022-23622-x.

[4] Roy, S., Sadhukhan, R., Ghosh, U. and Das, T.K., **2015.** Interaction studies between biosynthesized silver nanoparticle with calf thymus DNA and cytotoxicity of silver nanoparticles. *Spectrochimica Acta Part A: Molecular and Biomolecular Spectroscopy*, *141*, pp.176-184. doi: 10.1016/j.saa.2015.01.041.

[5] Javahershenas, R., Makarem, A. and Klika, K.D., **2024.** Recent advances in microwave-assisted multicomponent synthesis of spiro heterocycles. *RSC advances*, *14*(8), pp.5547-5565. https://doi.org/10.1039/D4RA00056K.

[6] Dhameliya, T.M., Donga, H.A., Vaghela, P.V., Panchal, B.G., Sureja, D.K., Bodiwala, K.B. and Chhabria, M.T., **2020.** A decennary update on applications of metal nanoparticles (MNPs) in the synthesis of nitrogen-and oxygen-containing heterocyclic scaffolds. *RSC advances*, *10*(54), pp.32740-32820. https://doi.org/10.1039/D0RA02272A.

[7] Abdullah, A.M., Dadoosh, S.A., Thani, M.Z. and Fahad, A.S., **2023.** Using metal oxide nanoparticles as catalyst in benzimidazoles synthesis. *Earthline Journal of Chemical Sciences*, *9*(1), pp.63-76. https://doi.org/.34198/ejcs.9123.6376.

[8] He, P., Chen, B., Huang, L., Liu, X., Qin, J., Zhang, Z. and Dai, W., **2022.** Heterogeneous manganese-oxide-catalyzed successive cleavage and functionalization of alcohols to access amides and nitriles. *Chem*, *8*(7), pp.1906-1927. https://doi.org/10.1016/j.chempr.2022.02.021.

[9] Wang, P., Zhang, S., Wang, Z., Mo, Y., Luo, X., Yang, F., Lv, M., Li, Z. and Liu, X., **2023.** Manganese-based oxide electrocatalysts for the oxygen evolution reaction: a review. *Journal of Materials Chemistry A*, *11*(11), pp.5476-5494. https://doi.org/10.1039/D2TA09039B.

[10] Kumari, S., Poonia, B., Vashisth, C., Rhakho, A., Kaushik, S., Chakraborty, A. and Kanoo, P., **2025.** Facile and Efficient Synthesis of Benzoxazoles and Benzimidazoles using a Lewis Acidic MOF Catalyst. *Dalton Transactions*. 54, pp. 10627-10639. https://doi.org/10.1039/D5DT00500K.

[11] Jia, X., Ma, J., Xia, F., Gao, M., Gao, J. and Xu, J., **2019.** Switching acidity on manganese oxide catalyst with acetylacetones for selectivity-tunable amines oxidation. *Nature Communications*, *10*(1), p.2338. https://doi.org/10.1038/s41467-019-10315-9.

[12] Manavalan, R.K., Enoch, K., Volegov, A.S., Angusamy, G. and Nallasivam, S., **2024.** Review on medical applications of manganese oxide (Mn^{2+}, Mn^{3+}, and Mn^{4+}) magnetic nanoparticles. *Journal of Nanomaterials*, *2024*(1), p.1073915., https://doi.org/10.1155/2024/1073915.

[13] Kong, Y., Jiao, R., Zeng, S., Cui, C., Li, H., Xu, S. and Wang, L., **2020.** Study on the synthesis of Mn_3O_4 nanooctahedrons and their performance for lithium ion batteries. *Nanomaterials*, *10*(2), p.367, https://doi.org/10.3390/nano10020367.

 © Ariston Publications 2025. All rights reserved.